



OPEN ACCESS

RECEIVED
4 February 2024REVISED
10 April 2024ACCEPTED FOR PUBLICATION
23 April 2024PUBLISHED
8 May 2024







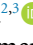









Original Content from
this work may be used
under the terms of the
[Creative Commons
Attribution 4.0 licence](#).

Any further distribution
of this work must
maintain attribution to
the author(s) and the title
of the work, journal
citation and DOI.



PAPER

Influence of source parameters on the longitudinal phase-space distribution of a pulsed cryogenic beam of barium fluoride molecules

M C Mooij^{1,2} , H L Bethlem^{1,3,*} , A Boeschoten^{2,3} , A Borschevsky^{2,3} , K Esajas^{2,3} , T H Fikkers^{2,3} ,
S Hoekstra^{2,3} , J W F van Hofslot^{2,3} , K Jungmann^{2,3} , V R Marshall^{2,3} , T B Meijknecht^{2,3} ,
R G E Timmermans^{2,3} , A Touwen^{2,3} , W Ubachs¹ , L Willmann^{2,3}  and Y Yin^{2,3,4} 

NL-eEDM collaboration

¹ Department of Physics and Astronomy, LaserLab, Vrije Universiteit Amsterdam, Amsterdam, The Netherlands² Nikhef, National Institute for Subatomic Physics, Amsterdam, The Netherlands³ Van Swinderen Institute for Particle Physics and Gravity, University of Groningen, Groningen, The Netherlands⁴ Present address: Department of Chemistry, University of Basel, Switzerland

* Author to whom any correspondence should be addressed.

E-mail: H.L.Bethlem@vu.nl**Keywords:** buffer gas cooled beam source, molecular beam, phase-space distribution, electric dipole moment of the electron

Abstract

Recently, we have demonstrated a method to record the longitudinal phase-space distribution of a pulsed cryogenic buffer gas cooled beam of barium fluoride molecules with high resolution. In this paper, we use this method to determine the influence of various source parameters. Besides the expected dependence on temperature and pressure, the forward velocity of the molecules is strongly correlated with the time they exit the cell, revealing the dynamics of the gas inside the cell. Three observations are particularly noteworthy: (1) The velocity of the barium fluoride molecules increases rapidly as a function of time, reaches a maximum 50–200 μs after the ablation pulse and then decreases exponentially. We attribute this to the buffer gas being heated up by the plume of hot atoms released from the target by the ablation pulse and subsequently being cooled down via conduction to the cell walls. (2) The time constant associated with the exponentially decreasing temperature increases when the source is used for a longer period of time, which we attribute to the formation of a layer of isolating dust on the walls of the cell. By thoroughly cleaning the cell, the time constant is reset to its initial value. (3) The velocity of the molecules at the trailing end of the molecular pulse depends on the length of the cell. For short cells, the velocity is significantly higher than expected from the sudden freeze model. We attribute this to the target remaining warm over the duration of the molecular pulse giving rise to a temperature gradient within the cell. Our observations will help to optimize the source parameters for producing the most intense molecular beam at the target velocity.

1. Introduction

Molecular radicals offer a number of unique possibilities for precision tests of fundamental physics theories [1–3] and quantum technology [4–7]. Traditionally, these molecules are created using ovens [8], resulting in samples at relatively high temperatures which are of limited use for these applications. Rotationally and translationally cold samples of radicals have been produced by entraining laser-ablated species in a supersonic expansion of a carrier gas. In this way bright, $>10^9$ molecules per steradian per pulse in a single rotational level, and short, $<20 \mu\text{s}$, beam pulses have been generated, see for instance [9] and references therein. The mean forward velocity of these beams is determined by the carrier gas and is typically around 600 m s^{-1} when using argon and 300 m s^{-1} for xenon [10].

A radically different approach for creating intense beams of molecules and molecular radicals is the so-called cryogenic buffer gas beam source, first introduced by Maxwell *et al* [11] and further developed by

Patterson and Doyle [12], van Buuren *et al* [13], Barry *et al* [14], Hutzler *et al* [15, 16] and others. In this method, molecules are introduced into a cold cell by a capillary [11–13, 17, 18], by laser ablation of a target containing a precursor [11, 12, 14, 15, 19–30] or by letting laser ablated atoms react with a donor gas [31–34]. The hot molecules are cooled by collisions with cold helium or neon buffer gas. After many collisions, a fraction of the molecules escapes the cell to form a molecular beam. The dimensions of the cell and the flow rate of the buffer gas determine the pressure within and are chosen in such a way that a significant fraction of the molecules is thermalized before hitting the wall of the cell. It was shown by Patterson and Doyle [12] that by operating the source at a high flow rate, the molecules are more efficiently extracted from the cell, resulting in a more intense molecular beam. At the same time, the higher flow rate leads to a supersonic boost at the exit of the cell, resulting in a faster molecular beam. Typical beam intensities above 10^{11} molecules per sr per pulse in a low rotational state have been reported with forward velocities below 170 m s^{-1} [14, 15]. In order to have an efficient extraction while avoiding a supersonic boost to occur, two-stage cryogenic buffer cells have been investigated [12, 19]. Truppe *et al* [31] introduced a cell design that was optimized for creating relatively short ($\sim 300 \mu\text{s}$) but intense molecular beams.

Over the last few years, we have constructed a pulsed cryogenic buffer gas cooled beam source that provides barium monofluoride (BaF) molecules for an experiment that will search for the electron's electric dipole moment (*eEDM*) [35]. In the experiment, the BaF molecules will be decelerated to below 30 m s^{-1} using a 4.5 m long travelling-wave Stark decelerator [36]. There is a trade-off between the deceleration strength and the acceptance of the decelerator [37]. In order to decelerate a reasonable fraction of the beam with the current setup, we need a bright beam with an initial velocity not too far above 200 m s^{-1} . Note that, the required length of the decelerator scales with the velocity squared; if the velocity of the initial beam would be 230 m s^{-1} instead of 200 m s^{-1} , we would need a decelerator with a length of 6 m, to have the same acceptance. Therefore, understanding what determines the velocity of our source and how the source can be optimized for slow beams is of the utmost importance.

Recently we have demonstrated a sensitive method to determine the forward velocity of a buffer gas cooled beam of barium fluoride molecules as a function of time after the ablation pulse, i.e. the longitudinal phase-space distribution of the beam, based on a two-step laser excitation scheme [38]. This method is similar to the one used by Barry *et al* [39] and Hemmerling *et al* [40] to study the velocity distribution of laser cooled beams of SrF and CaF, respectively. Here we present a detailed study of the phase-space distribution of a buffer gas cooled beam of barium fluoride as a function of various source parameters. Our paper is organized as follows: in section 2, we introduce our source in detail, followed by an explanation of the so-called sudden freeze model that predicts the dependence of the velocity on the temperature and pressure of the buffer gas, and a recap of our detection method. In section 3, we present measurements of the phase-space distributions while varying source parameters such as the power of the ablation laser, the repetition rate, the temperature of the cell, the flow rate of the SF₆, the operation time, the flow rate of the neon buffer gas and the cell length. Finally, in section 4, we summarize our findings.

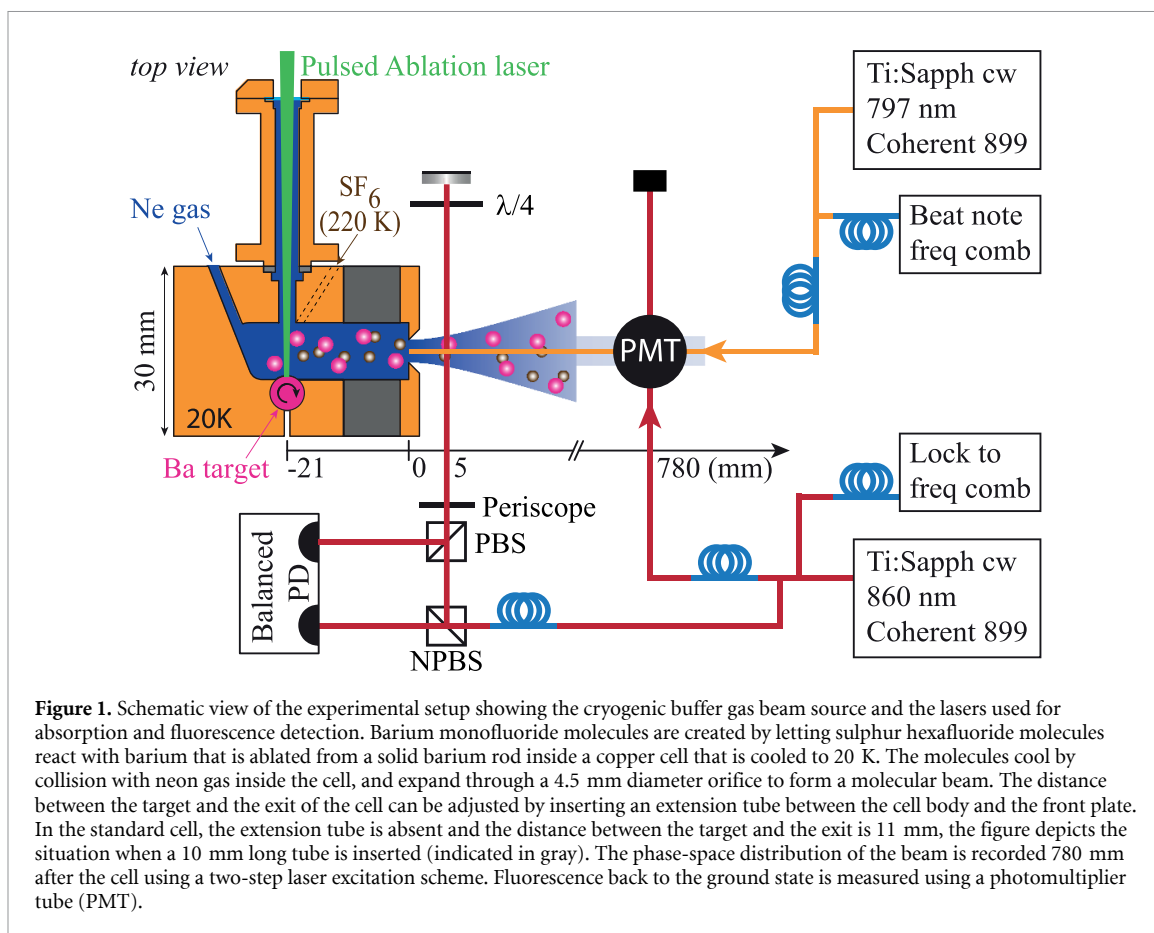
2. Method

2.1. Formation of the molecular beam

Figure 1 shows a schematic of our setup including a top-view of our cryogenic buffer gas beam source and the laser beam paths. The design of our cryogenic source is based on that of Truppe *et al* [31] and Esajas [33]. The heart of our setup is formed by a cubical copper cell kept at a temperature of around 20 K using a 2-stage cryo-cooler (Sumitomo Heavy Industries, cold head RP-082B2S). A continuous flow of pre-cooled neon is passed through the cell with a flow rate of 10–70 standard cubic centimeter per minute (sccm)⁵.

The beam of BaF molecules is formed in four steps: (i) Inside the cell, barium is ablated by a pulsed Nd:YAG laser (532 nm, 5 ns pulse, 10 Hz, typically 8 mJ per pulse measured outside the vacuum) from a rotating solid Ba target. (ii) The barium atoms react with sulphur hexafluoride (SF₆) molecules that are injected into the cell from a copper tube kept at a temperature of 220 K and with a flow rate of typically 0.03 sccm. (iii) The BaF molecules created in this reaction are cooled via collisions with neon atoms that is continuously flown through the cell with a flow rate of typically 20 sccm. (iv) They form a molecular beam by expanding through a 4.5 mm diameter orifice into the vacuum. The cell is surrounded by a copper and an aluminium heat shield, at temperatures of 6 K and ~ 30 K, respectively. These heat shields also provide the necessary pumping capacity to allow pressures on the order of 10^{-2} mbar inside the cell, while maintaining a pressure below 10^{-6} mbar in the molecular beam chamber. The typical values of the source parameters

⁵ 1 sccm = 4.48×10^{17} particles s⁻¹.



stated here are the *reference values*, which are used in all measurements presented below, unless a different value is explicitly mentioned.

2.2. Beam velocity as a function of pressure and temperature of the carrier gas

In this section, we will summarize some theory required to understand the dependence of the molecular beam velocity on the temperature and pressure of the buffer gas. If the source is operated at a very low buffer gas flow rate (for our cell well below 10 SCCM) and hence low density, the effusive regime prevails and the molecules leave the exit without colliding with the buffer gas. Consequently, the velocity distribution of the molecules in the beam reflects the temperature inside the cell, corresponding to 52 m s^{-1} for BaF molecules and 145 m s^{-1} for neon atoms. In practice, we use a much higher flow rate to ensure that the molecules are entrained in the buffer gas and are pumped out of the cell before they have a chance to diffuse to the cell walls. In this so-called hydrodynamic regime many collisions between neon atoms and BaF molecules occur while they leave the cell. As the pressure inside the cell is higher than outside, these collisions lead to a net force that accelerates the neon atoms and barium fluoride molecules along the beam axis and lowers the longitudinal velocity spread of the beam. In this situation, the velocity of the molecules in the beam depends both on the temperature of the cell and the density of the neon gas. To make this statement more quantitative, we summarize here a derivation to relate the temperature, velocity and flow rate, which is based on the derivations of Pauly [41] and Hutzler *et al* [15].

An isentropic expansion of a high-pressure gas into a vacuum leads to the conversion of internal energy into directed flow energy. In our case, the gas is composed of a mixture of the neon buffer gas, SF_6 and all molecules produced inside the cell, but since the neon accounts for over 99% of the gas, the beam is well described by an expansion of pure neon gas in which the molecules are taken along. When the distance from the source is large compared to the diameter of the exit of the cell, $z \gg d_{\text{exit}}$, the density in the beam, $n(z)$ decreases quadratically with distance:

$$n(z) \approx C \frac{n_0 d_{\text{exit}}^2}{z^2} \quad (1)$$

with n_0 the density in the cell and C is a constant that is ~ 0.25 for an effusive beam and ~ 0.15 for a supersonic beam [41]. The density in the cell is a function of the flow rate, f , the size of the aperture $A = \pi d_{\text{exit}}^2/4$, and the mean velocity of the beam, \bar{v} , and is given by [14]:

$$n_0 = \frac{4f}{A\bar{v}}. \quad (2)$$

The decrease in density is accompanied by an increase in the most probable velocity, $v_{\text{mp}}(z)$, and a decrease in the temperature, $T(z)$, along the beam. For a mono-atomic gas such as neon, it can be derived that [42]:

$$v_{\text{mp}}(z) = v_{\infty} \left[1 - \left(\frac{T(z)}{T_0} \right) \right]^{1/2} = v_{\infty} \left[1 - \left(\frac{n(z)}{n_0} \right)^{2/3} \right]^{1/2}, \quad (3)$$

with T_0 being the stagnation temperature of the gas in the cell. If all energy is converted, the temperature of the beam becomes zero, and the forward velocity becomes $v_{\infty}(T_0) = \sqrt{5k_B T_0/m}$, with m the mass of the buffer gas. In practice, the conversion process becomes increasingly slower while the density in the beam—and hence the collision rate—becomes smaller with distance from the exit of the cell. Consequently, the most probable velocity of the beam will be smaller than v_{∞} . In the so-called ‘sudden freeze’ model [41], it is assumed that the expansion stops abruptly at a certain distance from the source, from which point on the neon atoms and BaF molecules follow ballistic trajectories. The exact position, z_0 , of this ‘quitting surface’ is found by setting Z_2 , the integral over the remaining two-body collisions after passing this surface, equal to 1:

$$Z_2 = \int_{z_0/d_{\text{exit}}}^{\infty} dZ_2 = 0.0465 \sqrt{\frac{8}{\pi}} \bar{\sigma}_{\text{eff}} n_0 d_{\text{exit}}^{8/3} z_0^{-5/3} = 1, \quad (4)$$

with $\sigma_{\text{eff}, \text{b-b}}$ being the effective (temperature averaged) cross-section between buffer gas atoms. The numerical constant in the equation can be found from simulations [41], but its exact value is unimportant for our purpose. Combining the above equations with (2) that relates the density in the cell to the flow rate, f , we find:

$$v_{\text{mp}}(f, T_0) = v_{\infty}(T_0) \left[1 - a \left(\frac{f}{v_{\infty}(T_0)} \right)^{-4/5} \right]^{1/2}, \quad (5)$$

with $a = 0.33(\bar{\sigma}_{\text{eff}}/d_{\text{exit}})^{-4/5}$. This relation can be used to determine the temperature of the gas inside the cell, T_0 , from measurements of the mean velocity as a function of the flow rate⁶.

2.3. Detection

To monitor the performance of the source, the BaF molecules are detected using absorption directly behind the cell on the $X^2\Sigma^+ \rightarrow A^2\Pi_{1/2}$ transition using $\sim 1 \mu\text{W}$ of light at 860 nm in a 1 mm diameter beam. The absorption signal can be converted into an absolute number by taking into account the spatial and velocity distributions of the beam in the longitudinal and transverse directions, using a procedure that is similar to the one described by Wright *et al* [43]. At the reference settings the peak absorption is typically 10% (double pass), which corresponds to $1.9(6) \times 10^{10}$ BaF molecules in the $N = 0$ state per pulse and $1.3(5) \times 10^{11}$ molecules per sr per pulse. At a distance of 780 mm from the source, the molecules are excited by light from two Ti:Sapphire lasers (Coherent 899) that are referenced to a frequency comb. One of the lasers is aligned perpendicular to the molecular beam and is resonant with the $X^2\Sigma^+ \rightarrow A^2\Pi_{1/2}$ transition at 860 nm, while the other laser is aligned to be counter-propagating with respect to the molecular beam and resonant with the $A^2\Pi_{1/2} \rightarrow D^2\Sigma^+$ transition around 797 nm. The frequency of this second laser is red-shifted with respect to the transition frequency to compensate for the Doppler shift. From this detuning, we infer the longitudinal velocity of the molecules. More information on this method can be found in [38].

Once excited to the D -state, part of the molecules will decay back to the ground state by emitting a photon at 413 nm which is efficiently detected using a photomultiplier tube (PMT). A 40 nm wide band-pass filter around 400 nm is used to filter out scattered photons from the laser beams and unwanted fluorescence, resulting in a nearly background-free detection [44].

Figure 2 shows a typical measurement of the phase-space distribution reconstructed at the exit of the source [38]. In order to be able to compare phase space distributions taken at different settings, we sum the reconstructed velocity distribution at the exit of the cell over a time interval that increases from 2 μs at the

⁶ In this derivation, the flow velocity of the neon gas, which is 7–10 m s^{−1} in our experiments, is neglected.

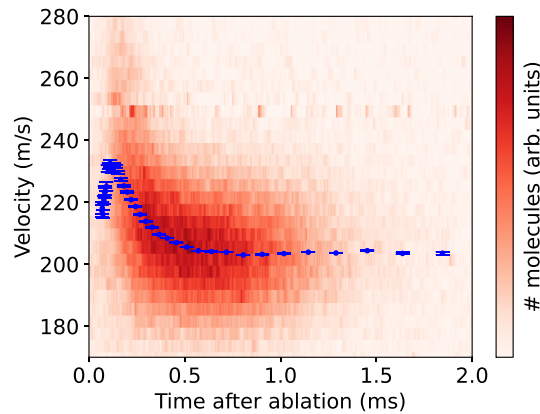


Figure 2. Phase-space distribution of the molecular beam reconstructed at the exit of the source. The blue data points represent the mean velocities resulting from a Gaussian fit to the data at specific times. The horizontal line observed at 250 m s^{-1} is due to difficulties in determining the frequency of the laser that drives the $A - D$ transition when its beat note with the frequency comb is equal to the repetition rate of the frequency comb.

beginning of the pulse to about $250 \text{ } \mu\text{s}$ at the end of the pulse and fit these with a Gaussian function. The mean velocity is shown as the blue data points that overlay the measured phase space distribution. The error bars represent the uncertainty from the fit.

3. Characterization of the cryogenic buffer gas beam source

In this section, we will discuss the dependency of the longitudinal phase-space distribution of the molecular beam on various source parameters in order to understand the dynamics within the cell. We will vary these parameters one at a time around the reference values. In section 3.1, we will study the influence of the ablation power, the repetition rate, the temperature of the cell and the flow rate of the SF_6 . In section 3.2, we will discuss the influence of the operation time. In section 3.3, we will discuss the influence of the neon flow rate and finally in section 3.4, we will investigate how the phase space distribution of the beam changes when the length of the cell is increased.

3.1. Influence of the ablation pulse energy and repetition rate, cell temperature and SF_6 flow rate

Figure 3(a) shows the mean velocity of BaF molecules as a function of time after the ablation pulse while using ablation pulse energies of 8 mJ (blue data points) and 4 mJ (red data points). As observed, the velocity first increases and reaches a maximum $\sim 0.1 \text{ ms}$ after the ablation pulse and then decreases. At 8 mJ, the velocity increases to above 250 m s^{-1} , whereas at 4 mJ, the velocity peaks at about 220 m s^{-1} . The number of molecules exiting the source is decreased by about a factor of 3 when the pulse energy is decreased from 8 mJ to 4 mJ.

The fact that the velocity of the molecules is lower in the trailing end of the molecular beam does not seem surprising, given that barium fluoride molecules are produced at very high temperatures [45] and require a minimum number of about 50 collisions [46] before being cooled by the cold neon buffer gas. Naively, we may expect that the molecules that exit the cell shortly after the ablation pulse have had less collisions and are faster than molecules that exit the cell later. This is however *NOT* what we see. Our measurements show that molecules leaving the cell immediately after the ablation pulse have comparable velocities to those at the tail of the pulse, while those that exit the cell $50\text{--}200 \text{ } \mu\text{s}$ after the ablation pulse, are faster. We deduce from this that, *at any time during the pulse*, the BaF molecules are in thermal equilibrium with the buffer gas. As the mean flow velocity of the buffer gas and BaF molecules are the result of the expansion of the gas inside the cell, the velocity reflects the initial temperature of the buffer gas inside the cell. The observed correlation between the velocity and time reflects the sharp increase in temperature of the buffer gas due to the hot ablation plume and the subsequent decrease in temperature via conduction to the walls and collisions with the cold neon gas that is continuously flown into the cell. This hypothesis is consistent with the $\sim 50 \text{ } \mu\text{s}$ thermalization time expected at the neon densities in our cell and also with earlier observations of Skoff *et al* [47]. Note that the cell body is not expected to heat up significantly by a single ablation pulse⁷, hence we conclude that the limiting factor is the heat conduction of the neon gas to

⁷ From the mass of the cell body and the heat capacity of copper at 20 K [48], we estimate that the temperature of the cell body increases by $\sim 5 \text{ mK}$ due to a single laser pulse with an energy of 8 mJ.

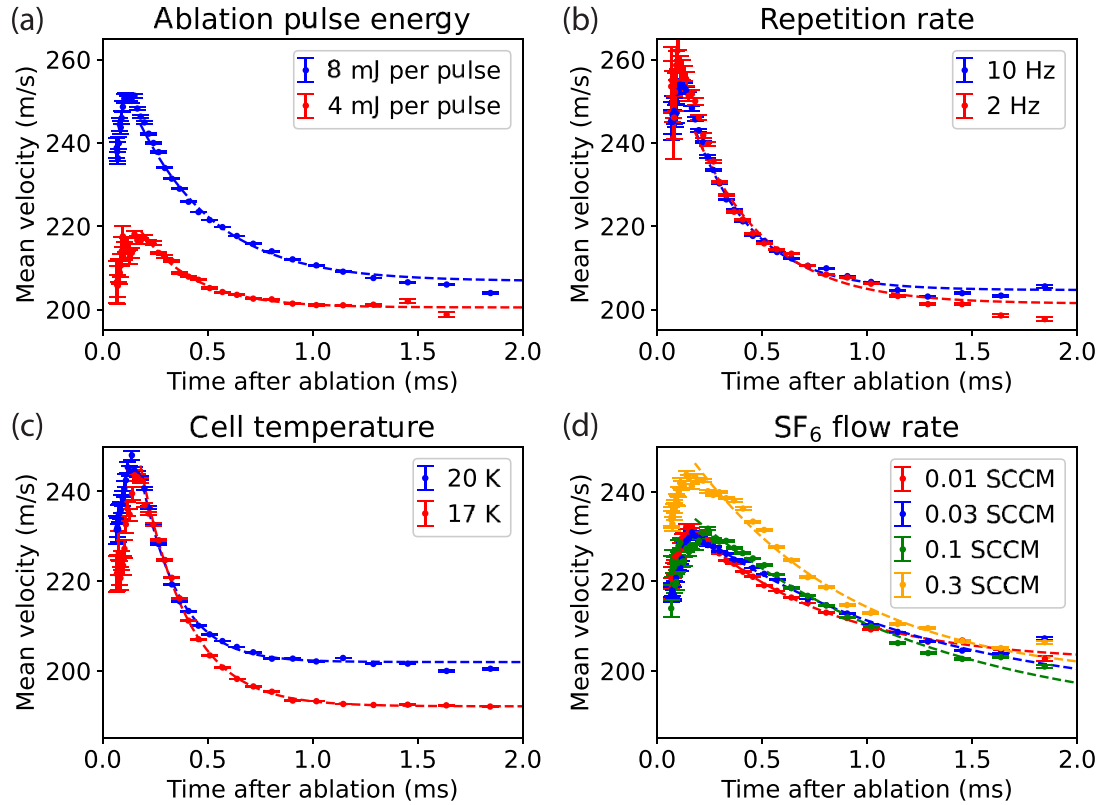


Figure 3. Mean velocity of the molecular beam as a function of time for different values of (a) the ablation pulse energy, (b) the repetition rate, (c) the cell temperature and (d) the SF_6 flow rate as indicated in the figure. All measurements are taken using a neon buffer gas flow rate of 20 SCCM. The blue data points in all sub-figures are different measurements taken at the reference settings. The dashed lines results from fits using (6).

the cell walls. This will be discussed further in section 3.2. It may be observed that even after 1.5 ms the mean velocity measured with an ablation energy of 8 mJ per pulse is still slightly higher than that measured with 4 mJ per pulse. We will come back to this difference in section 3.4.

Figure 3(b) shows the mean velocity of BaF molecules as a function of time measured at the same ablation energy of 8 mJ per pulse, but with a repetition rate of 10 Hz (blue data points) or 2 Hz (red data points). As expected, the measured velocities early in the pulse are very similar, but the velocity in the tail of the molecular pulse drops to a slightly lower velocity, indicating that the temperature of the cell may be slightly lower when operated at 2 Hz instead of 10 Hz.

Figure 3(c) shows the mean velocity of BaF molecules as a function of time measured when the copper cell is kept at 20 K (blue data points) or 17 K (red data points). Again, the measured velocities early in the pulse are very similar, but the velocity in the trailing end of the molecular pulse drops to a lower velocity when the cell is kept at a lower temperature. This shows that the source is ideally operated at the lowest possible cell temperature. The minimal temperature is determined by the requirement that the pressure anywhere in the system is above the vapor pressure of neon at that temperature. We observe that at a cell temperature below 20 K, the neon line becomes completely clogged within ~ 1 h, which we attribute to a small kink in the neon supply line.

Figure 3(d) shows the mean velocity of BaF molecules as a function of time measured when the SF_6 flow rate is varied from 0.01 SCCM to 0.3 SCCM. When the SF_6 flow rate is kept below 0.1 SCCM, the heat introduced by the SF_6 that is injected into the cell through a copper tube kept at a temperature of 220 K, is apparently negligible. Note that the number of barium fluoride molecules produced with these flow rates is similar.

If it is assumed that, after the initial rise, the temperature decreases exponentially, the velocity of the molecular pulse can be fitted to a simple exponential function of the form:

$$v(t) = \sqrt{v_f^2 + (v_i^2 - v_f^2) e^{-t/\tau}}, \quad (6)$$

with v_i and v_f being the initial and final velocities, respectively, and τ a characteristic time constant. These fits are shown as the dashed lines in figure 3. As may be observed, the fitted characteristic time constants between

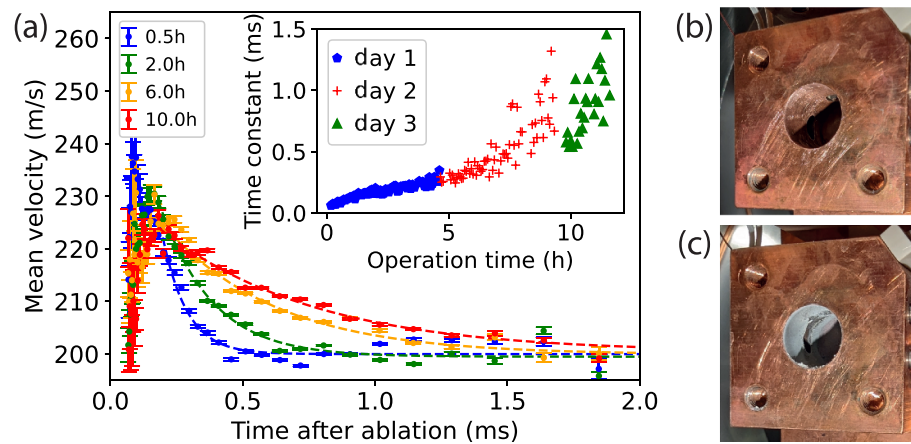


Figure 4. The effect of operation time. In (a), the mean velocity as a function of time is shown after operating the source for a time period as indicated. When the source is operated for extended times, the exponential decrease of the velocity becomes increasingly slower, resulting in a larger time constant as shown in the inset. (b) and (c) are two pictures of the cell with the front plate removed that are taken before and after measuring the data shown in (a), respectively. It is clear that the cell wall becomes covered with a substantial layer of dust.

the sets of measurements presented in panels (a)–(d) are rather different, which we blame on the cell being operated for extended times. In the next section, we will study this effect in more detail.

3.2. Influence of the operation time

In order to study the effect of the operation time, we thoroughly cleaned the copper cell using acetic acid and subsequently measured the phase space distribution at the same setting for 12 h distributed over three consecutive days. At the end of each day, the source was heated up to 295 K to remove particles that are frozen to the cell and heat shields. Figure 4(a) shows measurements taken after operating the source for 0.5–10 h. The dashed lines, also shown in the figure, are fits to the data using (6). The inset shows the resulting time constants from these fits as a function of operation time. During the approximately 12 h of operation, the measured time constant increased from below 100 μ s to above 1 ms, which we attribute to barium, barium-sulfides and other reaction products, covering the walls of the cell. This dust decreases the thermal conductivity between the cell and the neon buffer gas. Cleaning the cell resets the source, while simply heating the cell to remove neon and SF₆ ice, has no effect on the measured velocity distribution. Figures 4(b) and (c) show photographs of the cell without front aperture, taken before and after measuring the data shown in figure 4(a), respectively, clearly showing the contamination that builds up on the cell wall. The fact that the time constant changes during the operation of the source complicates the systematic study of the source considerably, forcing us to change parameters as quickly as possible while keeping an acceptable signal-to-noise ratio. Similar observations were made by Wright *et al* [43] in their experiments on AlF. Using NF₃ instead of SF₆ as a fluor donor, they observed the same yield but with a significantly slower cell degradation. In our experiments on BaF, NF₃ gave a significantly smaller yield and was not studied further.

3.3. Influence of the neon flow rate

In this section we will discuss the effect of the neon flow rate. Figure 5 shows the reconstructed phase-space distributions at the exit of the cell for buffer gas flow rates between 10 and 70 SCCM (a)–(g) along with the signal integrated over velocity (h) or time (i). Five trends are observed with higher flow rate: (i) the intensity and (ii) the pulse length of the molecular beam increase, as does the (iii) the characteristic time constant that describes the exponential decrease in temperature in the tail of the pulse. Furthermore, (iv) the mean velocity of the beam increases, while the (v) velocity spread decreases. The first two effects, which are most obvious from figure 5(h), are attributed to the increased diffusion time at higher neon densities, which reduces the loss of molecules frozen to the cell walls and leads to more efficient extraction from the cell. These effects have been discussed in detail by Patterson and Doyle [12]. The third effect is expected from the fact that the thermal diffusivity of the neon buffer gas decreases with increased density. Finally, the fourth and fifth effects are due to the beam becoming more supersonic when the neon density in the cell is increased and will be analyzed in more detail in the remainder of this section. Before doing this, there is one more observation worth noting. At higher flow rates, a dip in intensity is observed in the time of flight curves presented in figure 5(h) around 0.8 ms after the ablation pulse. We do not have a clear explanation for this effect yet.

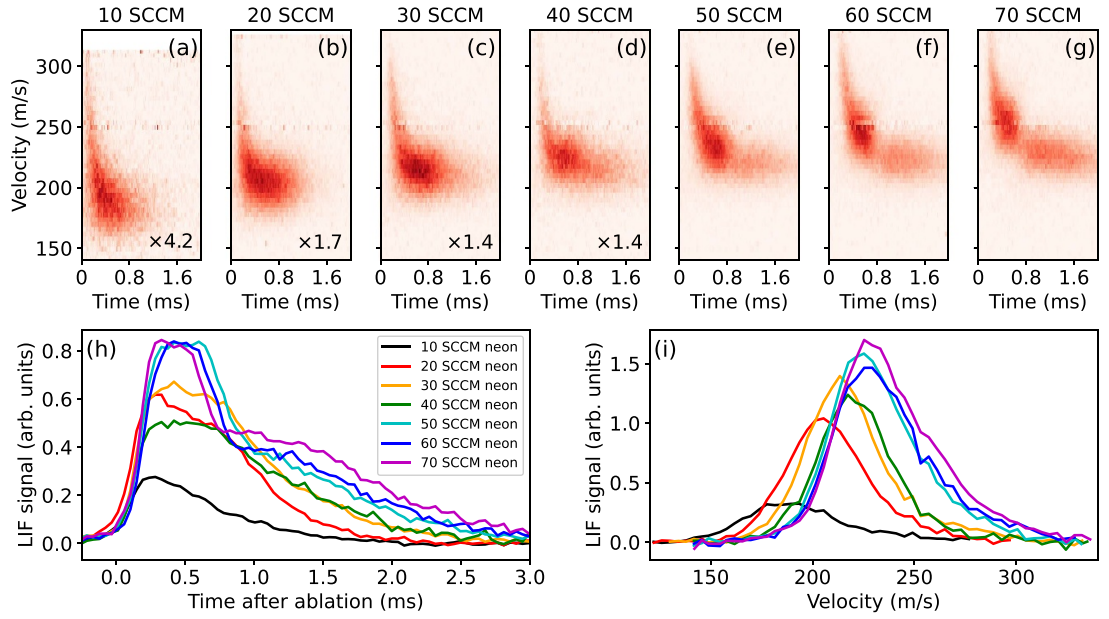


Figure 5. Phase-space distribution of the cryogenic beam for different neon flow rates. Panels (a)–(g) show the reconstructed phase-space distribution at the source exit, where $t = 0$ corresponds to the time that the ablation laser is fired. At low neon flow rates, the intensity has been multiplied with a factor as indicated in the panel. Panels (h) and (i) show the reconstructed intensity at different flow rates integrated over velocity and time, respectively. A number of trends are observed with higher flow rate, as described in the main text.

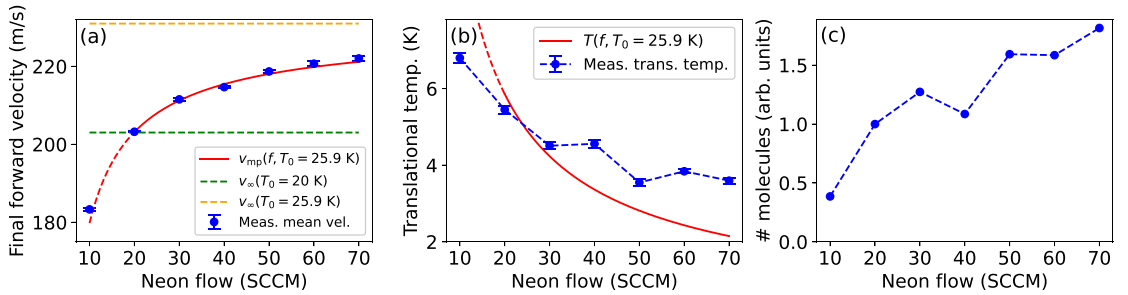


Figure 6. Velocity (a), temperature (b) and intensity (c) as a function of flow rate. (a) The blue data points show the final velocity, v_f , in the tail of the molecular beam as a function of the neon flow rate. The solid/dashed red line shows a fit of (5) to the data for flows between 20 and 70 SCCM from which we determine the terminal velocity v_{∞} , shown as the dashed orange line, and the temperature of the buffer gas, T_0 , which is 25.9 K in this case. For completeness, the green dashed line shows the expected terminal velocity at a cell temperature of 20 K. (b) The blue data points show the measured translational temperature, together with the prediction at 25.9 K. (c) Number of BaF molecules in the $X^2\Sigma^+$, $v = 0, N = 0, J = 1/2$ ground state.

As discussed in section 2.2, the mean velocity and translational temperature of the molecular beam depend on the temperature and pressure of the neon buffer gas inside the cell, which in turn depends on the neon flow rate. The blue data points in figure 6(a) show the final forward velocity, v_f , derived from fitting (6) to the mean velocity, as a function of time for each of the phase-space distributions presented in figures 5(a)–(g). The error bar of the data displays the uncertainty of this fit. The red solid line is a fit of (5) to this data from which we determine T_0 and the terminal velocity $v_{\infty}(T_0)$, shown as the orange dotted line⁸. In figure 6(b), the blue data points show the corresponding velocity spreads translated into a temperature. The solid red line shows the expected translational temperature from (3) at T_0 found from the fit to the data in (a). As may be observed, the model fits the measured mean velocities (and to a lesser extent) the translational temperature well, however, from the fit parameter, $v_{\infty}(T)$, we find that the buffer gas temperature in the tail of the molecular beam is 25.9 K, significantly above the temperature of the cell of 20 K. This is a somewhat surprising result, given that on these time scales the buffer gas appears to have reached thermal equilibrium with the walls, while from the measurements performed at lower repetition

⁸ From this fit we find a collision cross-section $\sigma_{\text{Ne-Ne}} = 1.9 \times 10^{-15} \text{ cm}^2$, which is slightly larger than found by a simple hard-sphere model: $\sigma_{\text{hs, Ne-Ne}} = 7.5 \times 10^{-16} \text{ cm}^2$ [41].

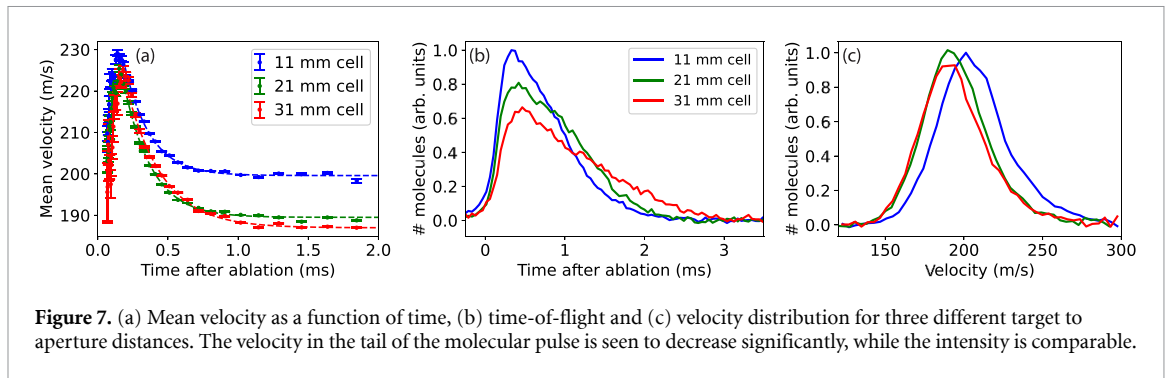


Figure 7. (a) Mean velocity as a function of time, (b) time-of-flight and (c) velocity distribution for three different target to aperture distances. The velocity in the tail of the molecular pulse is seen to decrease significantly, while the intensity is comparable.

rate, shown in figure 3(b), it is seen that the temperature of the cell returned (close) to its set value within 100 ms. We conclude from this that some part of the cell remains hot during the molecular pulse and only relaxes on a timescale 10–50 ms. We believe that it is in fact the barium target that remains hot. More evidence for this will be presented in the next section.

It would be insightful to determine the temperature of the buffer gas not only at the tail but at any time during the molecular beam pulse. However, this is complicated by the fact that the cooling rate towards the wall depends on the neon density in the cell and hence the flow rate. If we take the velocity measured at a flow rate of 70 SCCM to be the terminal velocity, we find that, at its peak, the temperature of the buffer gas is increased to about 40 K at an ablation pulse energy of 8 mJ/pulse. This is a lower limit for the temperature.

Figure 6(c) shows the brightness of the beam of barium fluoride molecules in the $X^2\Sigma^+, v=0, N=0, J=1/2$ ground state as function of the neon flow rate found by integrating the phase-space distributions shown in figures 5(a)–(g). As may be observed, the number of molecules increases by about a factor of 4.7 when the neon flow rate is increased from 10 to 70 SCCM. Note that, the sudden freeze model (presented in section 2.2) predicts that the intensity does not depend strongly on the neon flow rate, as the slight increase of the relative population in the $N=0$ state due to the lower rotational temperature at high neon flow rates, is compensated by a the increased divergence of the beam [14]. The observed intensity increase at higher flow rate is attributed to the increased efficiency in extraction of the molecules from the cell [12]. The fact that the forward velocity and intensity follow the same trend is a coincident.

3.4. Influence of the target to aperture distance

So far, all measurements presented in the paper were performed with the standard cell that has a distance of 11 mm between the ablation target and the source exit. In this section, we will study what happens when the cell is extended to 21 or 31 mm. Figure 7(a) presents the mean velocity as a function of time, while (b) and (c) present the intensity integrated over velocity or time, respectively. The ablation power, cell temperature, neon and SF₆ flow rates are set to the reference values. All measurement were taken after the cell was operated for 2 h. Increasing the target to aperture distance to 21 mm results in a longer molecular pulse that has a significantly lower velocity at the tail of the molecular pulse, while the number of molecules in the beam is comparable. Extending the cell further reduces the velocity but leads to a drop in the number of molecules by about 10 %. Note that, using (5) at 20 K and a neon flow rate of 20 SCCM, the expected mean velocity for molecules exiting our cell is 178 m s⁻¹.

We attribute the observed dependence of the velocity on the distance from target to aperture on the occurrence of a heat gradient in the cell. After the ablation pulse, the heat deposited in the ablated barium atoms is transferred to the buffer gas within 100 μ s and is subsequently cooled away by the cell within a few ms. On the other hand, the heat deposited in the barium rod is transferred to the buffer gas at a slower rate and the target remains at elevated temperatures during the entire molecular pulse. Increasing the distance between the target and the exit results in the neon gas at the exit being closer to the cell temperature and the molecular beam being slower. This effect also explains the observed dependence of the final velocity on the ablation power, as was discussed in section 3.1.

4. Conclusions

We presented measurements of the phase-space distribution of a cryogenic buffer gas beam of BaF. We observe a strong correlation of the mean forward velocity of the BaF molecules at the time they exit the source which is attributed to the neon buffer gas being warmed up by the plume of hot atoms released from the target by the ablation pulse and subsequently being cooled down via conduction to the cell walls. When the cell is operated for a longer period of time, the walls of the cell become covered with a layer of isolating

dust which increases the time constant associated with the exponentially decreasing temperature of the neon gas. The barium target remains at elevated temperatures on a much longer time scale, resulting in a higher mean velocity than expected from the sudden freeze model. This velocity can be lowered by extending the length of the cell. Some of the observations above have been reported before, but our new method to accurately measure the phase-space distribution of the beam in combination with the stability and reproducibility of our cell allowed us to analyze these effects in great detail. As optimization of the source amounts to a compromise between brightness and a low forward velocity, a good understanding of the heating processes is pivotal for an optimal choice of the source parameters. In future work, we plan to also study the effect of the size and shape of the cell exit.

Data availability statement

All data that support the findings of this study are included within the article (and any supplementary files).

Acknowledgments

The NL-*e*EDM consortium receives program funding (EEDM-166 and XL21.074) from the Netherlands Organisation for Scientific Research (NWO). We thank Johan Kos, Rob Kortekaas and Leo Huisman for technical assistance to the experiment, and Wander van der Meer for help during the experiments. We acknowledge fruitful discussions with Mike Tarbutt and Stefan Truppe in the design of the cryogenic source.

ORCID iDs

M C Mooij  <https://orcid.org/0000-0002-9577-4951>
H L Bethlem  <https://orcid.org/0000-0003-4575-8512>
A Boeschoten  <https://orcid.org/0000-0001-6691-6183>
A Borschevsky  <https://orcid.org/0000-0002-6558-1921>
K Esajas  <https://orcid.org/0000-0002-4943-0998>
T H Fikkers  <https://orcid.org/0009-0009-1709-9805>
S Hoekstra  <https://orcid.org/0000-0002-9571-4510>
J W F van Hofslot  <https://orcid.org/0000-0001-7596-0434>
K Jungmann  <https://orcid.org/0000-0003-0571-4072>
V R Marshall  <https://orcid.org/0000-0001-5500-2618>
T B Meijknecht  <https://orcid.org/0000-0002-3289-9773>
R G E Timmermans  <https://orcid.org/0000-0002-3734-4232>
A Touwen  <https://orcid.org/0000-0002-3690-2706>
W Ubachs  <https://orcid.org/0000-0001-7840-3756>
L Willmann  <https://orcid.org/0000-0001-7289-9439>
Y Yin  <https://orcid.org/0000-0001-7830-6059>

References

- [1] Safronova M S, Budker D, DeMille D, Kimball D F J, Derevianko A and Clark C W 2018 Search for new physics with atoms and molecules *Rev. Mod. Phys.* **90** 25008
- [2] Andreev V *et al* 2018 Improved limit on the electric dipole moment of the electron *Nature* **562** 355–60
- [3] Roussy T S *et al* 2023 An improved bound on the electron's electric dipole moment *Science* **381** 46–50
- [4] DeMille D 2002 Quantum computation with trapped polar molecules *Phys. Rev. Lett.* **88** 4
- [5] Ni K-K, Ospelkaus S, de Miranda M H G, Pe'er A, Neyenhuis B, Zirbel J J, Kotochigova S, Julienne P S, Jin D S and Ye J 2008 A high phase-space-density gas of polar molecules *Science* **322** 231–5
- [6] Blackmore J A *et al* 2019 Ultracold molecules for quantum simulation: rotational coherences in CaF and RbCs *Quantum Sci. Technol.* **4** 014010
- [7] Yu P, Cheuk L W, Kozryyev I and Doyle J M 2019 A scalable quantum computing platform using symmetric-top molecules *New J. Phys.* **21** 093049
- [8] Ramsey N F 1985 *Molecular Beams (Oxford Classic Texts in the Physical Sciences)* (Oxford University Press)
- [9] Aggarwal P *et al* 2021 A supersonic laser ablation beam source with narrow velocity spreads *Rev. Sci. Instrum.* **92** 33202
- [10] Tarbutt M R, Hudson J J, Sauer B E, Hinds E A, Ryzhov V A, Ryabov V L and Ezhov V F 2002 A jet beam source of cold YbF radicals *J. Phys. B: At. Mol. Opt. Phys.* **35** 5013–22
- [11] Maxwell S E, Brahms N, deCarvalho R, Glenn D R, Helton J S, Nguyen S V, Patterson D, Petricka J, DeMille D and Doyle J M 2005 High-flux beam source for cold, slow atoms or molecules *Phys. Rev. Lett.* **95** 173201
- [12] Patterson D and Doyle J M 2007 Bright, guided molecular beam with hydrodynamic enhancement *J. Chem. Phys.* **126** 154307
- [13] van Buuren L D, Sommer C, Motsch M, Pohle S, Schenk M, Bayerl J, Pinkse P W H and Rempe G 2009 Electrostatic extraction of cold molecules from a cryogenic reservoir *Phys. Rev. Lett.* **102** 033001
- [14] Barry J F, Shuman E S and DeMille D 2011 A bright, slow cryogenic molecular beam source for free radicals *Phys. Chem. Chem. Phys.* **13** 18936–47

- [15] Hutzler N R, Parsons M F, Gurevich Y V, Hess P W, Petrik E, Spaun B, Vutha A C, DeMille D, Gabrielse G and Doyle J M 2011 A cryogenic beam of refractory, chemically reactive molecules with expansion cooling *Phys. Chem. Chem. Phys.* **13** 18976–85
- [16] Hutzler N R, Lu H I and Doyle J M 2012 The buffer gas beam: an intense, cold and slow source for atoms and molecules *Chem. Rev.* **112** 4803–27
- [17] Patterson D, Rasmussen J and Doyle J M 2009 Intense atomic and molecular beams via neon buffer-gas cooling *New J. Phys.* **11** 055018
- [18] Singh V, Samanta A K, Roth N, Gusa D, Ossenbrüggen T, Rubinsky I, Horke D A and Küpper J 2018 Optimized cell geometry for buffer-gas-cooled molecular-beam sources *Phys. Rev. A* **97** 032704
- [19] Lu H I, Rasmussen J, Wright M J, Patterson D and Doyle J M 2011 A cold and slow molecular beam *Phys. Chem. Chem. Phys.* **13** 18986–90
- [20] Bulleid N E, Skoff S M, Hendricks R J, Sauer B E, Hinds E A and Tarbutt M R 2013 Characterization of a cryogenic beam source for atoms and molecules *Phys. Chem. Chem. Phys.* **15** 12299–307
- [21] Hummon M T, Yeo M, Stuhl B K, Collopy A L, Xia Y and Ye J 2013 2D magneto-optical trapping of diatomic molecules *Phys. Rev. Lett.* **110** 143001
- [22] Zhou Y, Grimes D D, Barnum T J, Patterson D, Coy S L, Klein E, Muentner J S and Field R W 2015 Direct detection of Rydberg–Rydberg millimeter-wave transitions in a buffer gas cooled molecular beam *Chem. Phys. Lett.* **640** 124–36
- [23] Santamaria L, Sarno V D, Natale P D, Rosa M D, Inguscio M, Mosca S, Ricciardi I, Calonico D, Levi F and Maddaloni P 2016 Comb-assisted cavity ring-down spectroscopy of a buffer-gas-cooled molecular beam *Phys. Chem. Chem. Phys.* **18** 16715–20
- [24] Li X, Xu L, Yin Y, Xu S, Xia Y and Yin J 2016 Rotational relaxation of fluoromethane molecules in low-temperature collisions with buffer-gas helium *Phys. Rev. A* **93** 063407
- [25] Straatsma C J E, Fabrikant M I, Doublerly G E and Lewandowski H J 2017 Production of carbon clusters C_3 to C_{12} with a cryogenic buffer-gas beam source *J. Chem. Phys.* **147** 124201
- [26] Bu W, Chen T, Lv G and Yan B 2017 Cold collision and high-resolution spectroscopy of buffer-gas-cooled BaF molecules *Phys. Rev. A* **95** 032701
- [27] Iwata G Z, McNally R L and Zelevinsky T 2017 High-resolution optical spectroscopy with a buffer-gas-cooled beam of BaH molecules *Phys. Rev. A* **96** 022509
- [28] Kozyryev I, Baum L, Matsuda K, Augenbraun B L, Anderegg L, Sedlack A P and Doyle J M 2017 Sisyphus laser cooling of a polyatomic molecule *Phys. Rev. Lett.* **118** 173201
- [29] Albrecht R, Scharwaechter M, Sixt T, Hofer L and Langen T 2020 Buffer-gas cooling, high-resolution spectroscopy and optical cycling of barium monofluoride molecules *Phys. Rev. A* **101** 013413
- [30] Shaw J C and McCarron D J 2020 Bright, continuous beams of cold free radicals *Phys. Rev. A* **102** 041302
- [31] Truppe S, Hambach M, Skoff S M, Bulleid N E, Bumby J S, Hendricks R J, Hinds E A, Sauer B E and Tarbutt M R 2018 A buffer gas beam source for short, intense and slow molecular pulses *J. Mod. Opt.* **65** 648–56
- [32] Xu S, Xia M, Gu R, Pei C, Yang Z, Xia Y and Yin J 2019 Cold collision and the determination of the $X^2\Sigma_1/2(v=1, N=1) \rightarrow A^2\Pi_1/2(v'=0, J'=1/2)$ frequency with buffer-gas-cooled MgF molecules *J. Quant. Spectrosc. Radiat. Transfer* **236** 106583
- [33] Esajas K 2021 Intense slow beams of heavy molecules to test fundamental symmetries *PhD Thesis* University of Groningen
- [34] Hofsäss S, Doppelbauer M, Wright S C, Kray S, Sartakov B G, Pérez-Ríos J, Meijer G and Truppe S 2021 Optical cycling of AlF molecules *New J. Phys.* **23** 075001
- [35] Aggarwal P et al 2018 Measuring the electric dipole moment of the electron in BaF *Eur. Phys. J. D* **72** 197
- [36] Aggarwal P et al 2021 Deceleration and trapping of SrF molecules *Phys. Rev. Lett.* **127** 173201
- [37] van de Meerakker S Y T, Bethlem H L, Vanhaecke N and Meijer G 2012 Manipulation and control of molecular beams *Chem. Rev.* **112** 4828–78
- [38] Mooij M C et al 2024 A novel method to determine the phase-space distribution of a pulsed molecular beam (arXiv:2401.16588)
- [39] Barry J F, Shuman E S, Norrgard E B and DeMille D 2012 Laser radiation pressure slowing of a molecular beam *Phys. Rev. Lett.* **108** 103002
- [40] Hemmerling B, Chae E, Ravi A, Anderegg L, Drayna G K, Hutzler N R, Collopy A L, Ye J, Ketterle W and Doyle J M 2016 Laser slowing of CaF molecules to near the capture velocity of a molecular MOT *J. Phys. B: At. Mol. Opt. Phys.* **49** 174001
- [41] Pauly H 2000 *Atom, Molecule and Cluster Beams I* vol 28 (Springer)
- [42] DePaul S, Pullman D and Friedrich B 1993 A pocket model of seeded supersonic beams *J. Phys. Chem.* **97** 2167–71
- [43] Wright S C, Doppelbauer M, Hofsäss S, Schewe H C, Sartakov B, Meijer G and Truppe S 2022 Cryogenic buffer gas beams of AlF, CaF, MgF, YbF, Al, Ca, Yb and NO — a comparison *Mol. Phys.* **121** e2146541
- [44] Murphree D H 2009 Nuclear spin-dependent parity nonconservation in diatomic molecules *PhD Thesis* Yale University
- [45] Davis G M, Gower M C, Fotakis C, Efthimiopoulos T and Argyrakis P 1985 Spectroscopic studies of ArF laser photoablation of PMMA *Appl. Phys. A* **36** 27–30
- [46] deCarvalho R, Doyle J M, Friedrich B, Guillet T, Kim J, Patterson D and Weinstein J D 1999 Buffer-gas loaded magnetic traps for atoms and molecules: a primer *Eur. Phys. J. D* **7** 289–309
- [47] Skoff S M, Hendricks R J, Sinclair C D J, Hudson J J, Segal D M, Sauer B E, Hinds E A and Tarbutt M R 2011 Diffusion, thermalization and optical pumping of YbF molecules in a cold buffer-gas cell *Phys. Rev. A* **83** 023418
- [48] Simon N J, Drexler E S and Reed R P 1992 *Properties of copper and copper alloys at cryogenic temperatures Final report* National Inst. of Standards and Technology (<https://doi.org/10.2172/5340308>)